Journal of Wind Engineering & Industrial Aerodynamics 242 (2023) 105576

Contents lists available at ScienceDirect

Journal of Wind Engineering & Industrial Aerodynamics

journal homepage: www.elsevier.com/locate/jweia

Non-Gaussian buffeting analysis of large structures by means of a Proper Orthogonal Decomposition

M. Esposito Marzino, V. Denoël *

Structural & Stochastic Dynamics, Structural Engineering Division, University of Liège, Liège, Belgium

ARTICLE INFO

Keywords:
Bispectral analysis
Complete cubic combination
Cubic root of the sum of the cubes

ABSTRACT

Proper Orthogonal Decomposition is implemented in a Bispectral Stochastic Analysis of large MDOF structures. Although Higher Order Stochastic Analysis has been introduced few decades ago, its establishment has found place only in a theoretical way, or applied to very small systems. Its heavy computational cost as well as resource consumption burden has let it aside for practical civil engineering applications. Nevertheless, in wind engineering, the community is increasingly considering the importance of non-Gaussian nature of wind induced vibrations. This is of interest for the extreme value analysis, for which many theoretical and empirical models exist for non-Gaussian random processes. In this context, a (bi-)spectral approach is realized in a 2-D frequency space where the bispectrum is computed then the 3rd statistical moment is obtained by means of a twofold integration. These operations are quite heavy as soon as the dimension of the problem increases. A novel algorithm implementation is proposed. It hinges on (i) the use of Proper Orthogonal Decomposition and the (ii) development of an optimized numerical method. The proposed algorithmic arrangement minimizes the number of operations, and consequently saves time and memory, while conserving precision in estimating 3rd order statistical moments of structural responses.

1. Introduction

Wind Engineering, as we know it today, is a fairly young discipline from the 1950's (Davenport, 1961; Isyumov, 2012). It is a quite complex topic, collecting more general disciplines such as meteorology, fluid dynamics and structural dynamics, among others. Random vibrations resulting from wind loads on structures can be tackled either in time domain or in frequency domain (Mircea, 1995). These two approaches are more or less appropriate depending on the features of the problem under consideration. For example, in transient winds such as tornadoes, downbursts, typhoons, Kareem and Wu (2013), Solari and De Gaetano (2018) and Solari (2020), or in case of highly nonlinear systems, time domain analysis is preferred since it is much more capable of capturing these time-varying behaviors (Augusti et al., 1986; Aas-Jakobsen and Strømmen, 2001; Carassale and Solari, 2002; Gusella and Materazzi, 2000). On the other hand, linear systems under stationary excitations are much better studied in the frequency domain (Fan et al., 2022; Denoël et al., 2023), allowing for a clearer comprehension of the physical system-excitation interaction. This is even more important as soon as non Gaussian features of the loading and response need to be captured, at third order (Fan et al., 2022; Denoël et al., 2023; Denoël, 2011) or even fourth order (Denoël, 2012; Trapp and Wolfsteiner, 2019). Nonetheless, it should be noted that the non linearity of the loading or structural response does not hinder usage of spectral methods (Denoël and Carassale, 2014) and the possible use of a spectral approach. Therefore, the domain of application of spectral approaches, as the one followed in this paper, should not be underestimated.

In wind engineering, however, wind loads resulting from wind pressures in the Atmospheric Boundary Layer (ABL) are often assumed to be Gaussian stationary random processes (Kareem and Wu, 2013). This reflects the fact that a second order buffeting analysis is typically handled by a spectral analysis, which can be summarized as the Power Spectral Density (PSD) of the structural response obtained with application of the known Davenport Chain (Isyumov, 2012). This approach has analytical advantages since, in case of linear mechanical structural behavior, the structural response happens to be Gaussian too, so it can be fully characterized by the first two statistical moments only (Mircea, 1995; Gusella and Materazzi, 2000, 1998; Gioffrè et al., 2001), mean and variance. When the non linearity concerns the aerodynamic nature of loading, the solution is complemented by a bispectral analysis (Gusella and Materazzi, 2000, 1998) which allows the determination of the third statistical moments of the structural responses. Indeed, the stochastic approach would require the evaluation of an infinite number of higher-order statistical moments in order to properly characterize

* Corresponding author.
E-mail addresses: michele.espositomarzino@uliege.be (M. Esposito Marzino), v.denoel@uliege.be (V. Denoël).

https://doi.org/10.1016/j.jweia.2023.105576
Received 15 April 2023; Received in revised form 15 September 2023; Accepted 22 September 2023
Available online 16 October 2023

and quantify the divergence of the Probability Density Function (PDF) of the structural response from a Gaussian-like one, when a closed form expression of such a PDF cannot be determined (Benfratello et al., 2000), which inevitably increases the complexity in conceptual as well as practical terms.

Nonetheless, even though the non-Gaussian nature of the wind loading has been known for some times (Gurley et al., 1997), it is very seldom taken into account. Indeed, for common structures subjected to wind, due to the low turbulence intensity of common winds, the effects of the nonlinear loading terms on most of the civil structures might be neglected compared to the mean and linear terms (Benfratello et al., 1996). However the non-Gaussianity becomes more important as turbulence intensity grows (Holmes, 1981), but also because the nonlinear transformation of wind velocities into wind pressures (in the quasi-steady approach) results in an increase of energy in higher frequencies (Kareem, 1984). Hence, there might be cases in which neglecting the quadratic term can lead to significant overestimations/underestimations of the extreme values of the system's response.

Besides, many mathematical tools have been developed starting from the mid 19th century, for dealing with statistics related (i.e. random) problems. Among others, data reduction techniques play a significant role in many fields of engineering. Solari et al. presented the evolution of these mathematical tools (Solari et al. (2007)), in a general context, as well as applied to the main macro subjects concerning modern Wind Engineering. In particular, this work hinges on the concept of Proper Orthogonal Decomposition (POD) that has been extensively used in the early 2000s and widely applied well beyond Wind Engineering related problems. Interested readers can refer to Solari et al. (2007) for better insights.

In this paper, a stationary non-Gaussian wind turbulent load is assumed, whose statistical description is known in a probabilistic sense. Nevertheless, the concepts and developments that will be presented are as general as possible, thus applicable to similar case studies in which the same assumptions are satisfied, for instance when wind loads are combined with wave loading (Geuzaine and Denoël, 2019) or in other applications falling outside the classical scopes of wind engineering, such as fatigue analysis (Rizzi et al., 2011) where occurrence of high intensity peak responses (attributable to non-Gaussian response) can cause detrimental damages. Therefore, the work presented here aims at becoming a solid base for a practical methodology for Bispectral Stochastic Analysis (BSA) of large MDOF systems, by means of both mathematical and algorithmic tools.

2. Problem statement

In a buffeting analysis, the governing equations of motion read

$$\mathbf{M}\ddot{\mathbf{x}}(t) + \mathbf{C}\dot{\mathbf{x}}(t) + \mathbf{K}\mathbf{x}(t) = \mathbf{f}(t) \tag{1}$$

where $\mathbf{M}$, $\mathbf{C}$, $\mathbf{K}$ are the mass, damping, stiffness structural matrices, $\mathbf{x}(t)$ the structural response vector, and $\mathbf{f}(t)$ the vector of buffeting loads, at time instant t.

In the following developments, an arbitrarily large MDOF linear structure is considered, having a number NN of nodes, for a total of NDOFS Degrees-Of-Freedom (DOFs), meaning that NDFN = NDOFS/NN degrees-of-freedom per (structural) node have been considered. In following derivations, the concept of (aerodynamic) node will be extensively used. It corresponds to a set of points in a portion of space where the studied structure is located. The wind field is discretized at these nodes. For simplicity, they are assumed to match the nodes of the structural model, otherwise any interpolation technique can be used. While degrees-of-freedom are central in the finite element approach, nodes are the key elements of the loading model.

For the structural analysis, it is convenient to project Eq. (1) into the modal basis $\mathbf{\Phi}$ composed of a number NM of modes. Assuming a proportional structural damping $\mathbf{C}$, e.g. Rayleigh damping model, the linear system decouples into NM independent equations:

$$\mathbf{M}^\star\ddot{\mathbf{q}}(t) + \mathbf{C}^\star\dot{\mathbf{q}}(t) + \mathbf{K}^\star\mathbf{q}(t) = \mathbf{p}(t) \tag{2}$$

where $\mathbf{M}^\star = \mathbf{\Phi}^T\mathbf{M}\mathbf{\Phi}$, $\mathbf{C}^\star = \mathbf{\Phi}^T\mathbf{C}\mathbf{\Phi}$, $\mathbf{K}^\star = \mathbf{\Phi}^T\mathbf{K}\mathbf{\Phi}$ are the diagonal modal mass, damping and stiffness matrices, $\mathbf{q}(t)$ the modal responses, and $\mathbf{p}(t) = \mathbf{\Phi}^T\mathbf{f}(t)$ the vector of modal loads, at time t. Eq. (2) is transformed in its frequency domain counterpart, by taking its Fourier Transform,

$$\mathbf{Q}(\omega) = \mathbf{H}(\omega)\mathbf{P}(\omega) \tag{3}$$

where

$$\mathbf{H}(\omega) = \left(-\mathbf{M}^\star\omega^2 + \mathrm{i}\omega\mathbf{C}^\star + \mathbf{K}^\star\right)^{-1} \tag{4}$$

is the Frequency Response Function. Then, following standard spectral analysis (Lutes and Sarkani, 2004), the power spectral density of modal responses in given by

$$\mathbf{S}_Q(\omega) = \mathbf{H}(\omega)\mathbf{S}_P(\omega)\mathbf{H}^*(\omega) \tag{5}$$

where $\mathbf{S}_P(\omega)$ represents the power spectral density of modal forces $\mathbf{p}(t)$, and where the symbol $[\cdot]^*$ represents the conjugate transpose operator (not to be confused with $[\cdot]^\star$ which is used to indicate a modal quantity). The frequency response function is assumed diagonal, so that each element of $\mathbf{S}_Q(\omega)$ can be written

$$S_{Q_{mn}}(\omega) = H_m(\omega)H_n^*(\omega)S_{P_{mn}}(\omega). \tag{6}$$

In case of non proportional damping, precisely such as the one resulting from wind loading, the frequency response function might be fully populated with small elements outside the diagonal. In that case, modal coupling can be treated by considering an additional equivalent loading on the same uncoupled modal basis (Denoël and Degée, 2009; Canor et al., 2012), so that this assumption is not really a limitation for the following derivation. Integration along frequencies of Eq. (5) gives the second order statistical moment, namely variance (covariance) for auto- (cross-) elements of the 2D matrix of PSDs of modal responses $\mathbf{S}_\mathbf{Q}(\omega)$:

$$\Sigma_\mathbf{Q} := \mathbf{m}_{2,Q} = \int_{-\infty}^{\infty}\mathbf{S}_Q(\omega)\mathrm{d}\omega. \tag{7}$$

It is written $\mathbf{m}_{2,Q}$ to simplify later extension to higher orders. The diagonal elements of $\mathbf{m}_{2,Q}$ contain the variances of modal responses, $m_{2,Q_{mm}} = \sigma^2_{Q_m}$, and off-diagonal elements contain the covariances of modal responses which are important to keep track of the existing correlation between modal responses and allow accurate estimation of any quantity based on combinations thereof.

At third order, similar equations exist to express the bispectrum of modal responses $B_{Q_{mno}}(\omega_1,\omega_2)$, as a function of the bispectrum of modal loads,

$$B_{Q_{mno}}(\omega_1,\omega_2) = H_m(\omega_1)H_n(\omega_2)H_o^*(\omega_1+\omega_2)B_{P_{mno}}(\omega_1,\omega_2). \tag{8}$$

Integrating Eq. (8) for each combination (m,n,o) of natural vibration modes, it is possible to retrieve the 3D matrix of third order cross-moments, whose elements are given by

$$m_{3_{Q_{mno}}} = \iint_{-\infty}^{\infty} B_{Q_{mno}}(\omega_1,\omega_2)d\omega_1 d\omega_2. \tag{9}$$

Then, by combining Eqs. (7) and (9), we can define

$$\gamma_{3,Q_{mno}} = \frac{m_{3_{Q_{mno}}}}{\sigma_{Q_m}\sigma_{Q_m}\sigma_{Q_o}}. \tag{10}$$

When $m = n = o$, this quantity corresponds to the skewness coefficient of modal responses. It extends the concept to elements outside the main diagonal $m = n = o$.

There are two major challenges in the higher order spectral analysis:

- to compute the power spectral density $\mathbf{S}_P(\omega)$ and, more importantly here, the bispectrum $\mathbf{B}_P(\omega_1, \omega_2)$ of modal loads in an efficient way,
- to compute the integrals in Eqs. (7) and (9) in an efficient way.

This paper addresses these two challenges. Before detailing how data reduction techniques can be used to tackle the first issue, some more information is given in the following Section about the origin of non-Gaussianity in aerodynamic wind loads and how these features can be handled in a convenient model.

3. A general nonlinear polynomial aerodynamic loading model

There exist several quasi-steady models to express the aerodynamic wind loads at Degree-Of-Freedom (DOF) i of node I as a function of the average wind velocity $\overline{U}_I$ at that node and $u_I(t)$, $v_I(t)$, $w_I(t)$, the *elementary* velocity components of wind turbulence at the same node. The question of unsteady or self-excited forces is not addressed in this paper, so that aerodynamic damping, and possibly stiffness, are assumed as constant and are integrated in the structural matrices (Simiu and Scanlan, 1996). The family of quasi-steady models only is considered, where applied loads are expressed as memoryless transformations of the turbulence components. In this family, the fluctuating components $v_I(t)$ of the wind velocity are separated from the average values which are dealt with in a separate static analysis. For this reason, in the following, developments will neglect the presence of this mean component $\overline{U}_I$.

In traditional linear aerodynamic models, the fluctuating component of the aerodynamic loads at all DOFs are given by

$$\mathbf{f}(t) = \sum_{I=1}^{\mathtt{NN}} \mathbf{a}_I^{(u)} u_I(t) + \sum_{I=1}^{\mathtt{NN}} \mathbf{a}_I^{(v)} v_I(t) + \sum_{I=1}^{\mathtt{NN}} \mathbf{a}_I^{(w)} w_I(t) \tag{11}$$

where $\mathbf{f}(t)$ is a $\mathtt{NDOF} \times 1$ vector of loads at all DOFs of the structural model, which expresses that loads at all DOFs are obtained as linear combinations of elements velocity components of the turbulence at all nodes of the structure. In practice, the three vectors $\mathbf{a}_I^{(u)}$, $\mathbf{a}_I^{(v)}$ and $\mathbf{a}_I^{(w)}$ are mostly composed of zeroes since, in a finite element approach, the loads at the different DOFs of a given node are obtained by integration of the applied loads on elements connected to that node only. However, this notation is efficient; it resembles the localization operation in a standard finite element approach.

To simplify later notations, we use $v_{Ia}(t)$ to refer to the ath fluctuating component at node I, for instance $v_{I1}(t) = u_I(t)$. In a very general way, the wind loads at all DOFs are given by

$$\mathbf{f}(t) = \sum_{I=1}^{\mathtt{NN}} \sum_{a=1}^{\mathtt{NDEGW}} \mathbf{a}_{Ia} v_{Ia}(t) \tag{12}$$

where $\mathbf{a}_{Ia}$ collects the $\mathtt{NDOF}$ wind loading coefficients translating the influence of the ath fluctuating component at node I on the load at all DOFs. The summation on a, limited to $\mathtt{NDEGW}$, is discussed in the sequel. It is possible to see v_{Ia} as an element of matrix $\boldsymbol{v}$ whose size is $\mathtt{NN} \times \mathtt{NDEGW}$. This matrix can be partitioned in two different ways

$$\boldsymbol{v} = \left(\boldsymbol{v}_{:,1}, \boldsymbol{v}_{:,2}, \dots, \boldsymbol{v}_{:,a}, \dots, \boldsymbol{v}_{:,\mathtt{NDEGW}}\right) = \left(\hat{\boldsymbol{v}}_1, \hat{\boldsymbol{v}}_2, \dots, \hat{\boldsymbol{v}}_a, \dots, \hat{\boldsymbol{v}}_{\mathtt{NDEGW}}\right) \tag{13}$$

$$\boldsymbol{v} = \left(\boldsymbol{v}_{1,:}^T, \boldsymbol{v}_{2,:}^T, \dots, \boldsymbol{v}_{I,:}^T, \dots, \boldsymbol{v}_{\mathtt{NN},:}^T\right)^T = \left(\boldsymbol{v}_1, \boldsymbol{v}_2, \dots, \boldsymbol{v}_I, \dots, \boldsymbol{v}_{\mathtt{NN}}\right), \tag{14}$$

i.e. by lines or columns. The symbol $\boldsymbol{v}_{:,1}$ means all lines of the first column, while $\boldsymbol{v}_{1,:}^T$ all columns of the first line. We have also introduced the notation $\hat{\boldsymbol{v}}_a = \boldsymbol{v}_{:,a}$, as well as $\boldsymbol{v}_I = \boldsymbol{v}_{I,:}^T$.

The wind loading coefficients $\mathbf{a}_{Ia}$ are expressed as a function of the aerodynamic shape of the elements, as well as their orientation with the mean wind flow (Kimura and Tanaka, 1992; Janjic and Pircher, 2004; da Costa et al., 2022). In many models, the loads at a given DOF of a node I of the finite elements model are expressed as a function of the components of wind velocity $\boldsymbol{v}_{I,:}(t)$ at the same node I (of the wind field). Some more advanced models could result in forces at a given node that are also expressed as a function of the wind velocity at neighboring nodes (Denoël and Maquoi, 2012), which would increase the number of non-zero elements in $\mathbf{a}_{i,I}$ while offering the chance to increase the size of finite elements and reduce the total number of DOFs. In the following, no hypothesis is made on how $\mathbf{a}_{Ia}$ is constructed so that any memoryless wind loading model can be considered. Along the same line, a possible improvement of Eq. (12) would be to use a low-pass filter corresponding to the so-called numerical admittance, related to the discretization of the pressure field along elements into nodal values (Denoël and Maquoi, 2012). Although this is not included in the following developments, nothing hinders its consideration.

Based on these arguments, the establishment of coefficients $\mathbf{a}_{i,I}$ is more or less involved, depending on the fact that the studied structure is a line-like structure (Kimura and Tanaka, 1992), a large structure in a 2-D plane or even a large 3-D structure (Scanlan, 1993; da Costa et al., 2022). Many wind load models are linearized, so that $\boldsymbol{v}_{:,1} = \mathbf{u}$, $\boldsymbol{v}_{:,2} = \mathbf{v}$, $\boldsymbol{v}_{:,3} = \mathbf{w}$, i.e. nothing but the set of the three *elementary* wind components, or

$$\boldsymbol{v}_I(t) = \left(u_I(t), v_I(t), w_I(t)\right). \tag{15}$$

By linear wind load model, we mean that the smallness of the turbulence components with respect to the average wind velocity is considered and a series expansion is developed to obtain a linear relation between turbulence components and the wind loads. In more general models, the wind loading can be replaced by a polynomial expression of any arbitrary degree d. In the linear case, $d = 1$ and the number of wind components $\mathtt{NDEGW} = 3$. When the quadratic nature (Kareem et al., 1998; Denoël, 2009) of the loading is taken into account, $d = 2$, the set of wind components at a given node is extended to

$$\begin{aligned}&\boldsymbol{v}_I(t)\\ &= \left(u_I(t), v_I(t), w_I(t), u_I^2(t), v_I^2(t), w_I^2(t), u_I(t)v_I(t), u_I(t)w_I(t), v_I(t)w_I(t)\right)\end{aligned} \tag{16}$$

where all possible combinations of the components of wind velocity up to second degree have been considered, for a total of $\mathtt{NDEGW} = 9$ wind components. Higher degree models could also be envisaged by including turbulence loading components such as $u_I^3(t)$. The number of new elements when adding the terms of degree d is given by $(d+2)(d+1)/2$ (3 new terms for $d = 1$, 6 new terms for $d = 2$, 10 new terms for $d = 3$, etc.) so that, in total,

$$\mathtt{NDEGW} = \frac{1}{6}(d+1)(d+2)(d+3) - 1 \tag{17}$$

if terms up to degree d are kept. All in all, in the most generic format, the aerodynamic loads on the structure are therefore expressed by Eq. (12) where summations are performed on all aerodynamically loaded nodes (I) and all components of the wind load (a) which could be more than just three in case of nonlinear aerodynamic models.

By choosing to embed (to the authors' knowledge for the first time) all possible combinations of the various degrees of the elementary components, we give a very general meaning to Eq. (12). Indeed, although $\mathbf{f}(t)$ is written as a linear transformation of $\boldsymbol{v}(t)$, it is possible to include nonlinear memoryless transformations of the turbulence components up to any desired order. This model extends the linear formulation used by the scientific community so far. This expression is however significantly different: it conserves the properties of linear combinations (step II to III in Fig. 1), but it combines wind components that are themselves obtained as (possibly nonlinear) polynomial transformations of the elementary turbulence components (step I to II in Fig. 1).

In most of today's applications, *linear* wind load models are considered ($d = 1$) and, since the elementary wind turbulence components $u(t)$, $v(t)$, $w(t)$ are zero-mean Gaussian random processes (Simiu and Scanlan, 1996), vector $\boldsymbol{v}(t)$ is composed of Gaussian processes only and the wind forces are Gaussian processes as well. However, as soon as quadratic components are included in the loading model as in Eq. (16),

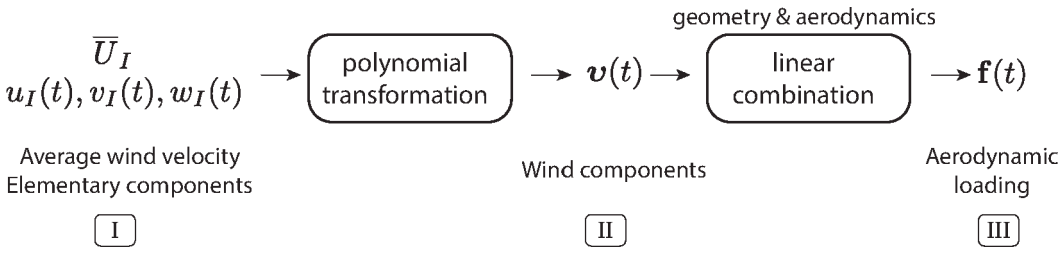

Fig. 1. Schematic of the general nonlinear polynomial aerodynamic loading model.

some wind turbulence components such as $u^2(t)$ are no longer Gaussian, and so is the resulting loading.

Since the transformation II to III in the model is always linear, see Fig. 1, the determination of the statistics of $\mathbf{f}(t)$ as a function of those of $\boldsymbol{v}(t)$ is straightforward. Hence, the main objective of the general model is to derive the statistics of $\boldsymbol{v}(t)$, knowing those of the wind velocities $u_I(t)$, $v_I(t)$ and $w_I(t)$, which are assumed to be zero-mean and Gaussian. Therefore, the complete probabilistic description of all components $\boldsymbol{v}(t)$ can be expressed as a function of the (cross-)correlation functions of $u_I(t)$, $v_I(t)$ and $w_I(t)$ or, alternatively, of their (cross-)power spectral densities. In particular, considering the block representation in Eq. (13), the correlation matrix of the wind components takes the form

$$\mathbf{R}_{\hat{\boldsymbol{v}}}(\Delta t) = \begin{pmatrix} \mathbf{R}_{\hat{v}_{11}}(\Delta t) & \mathbf{R}_{\hat{v}_{12}}(\Delta t) & \cdots & \mathbf{R}_{\hat{v}_{1,\mathrm{NDEGW}}}(\Delta t) \\ \mathbf{R}_{\hat{v}_{21}}(\Delta t) & \mathbf{R}_{\hat{v}_{22}}(\Delta t) & & \mathbf{R}_{\hat{v}_{2,\mathrm{NDEGW}}}(\Delta t) \\ \vdots & & & \\ \mathbf{R}_{\hat{v}_{\mathrm{NDEGW},1}}(\Delta t) & \mathbf{R}_{\hat{v}_{\mathrm{NDEGW},2}}(\Delta t) & & \mathbf{R}_{\hat{v}_{\mathrm{NDEGW},\mathrm{NDEGW}}}(\Delta t) \end{pmatrix} \tag{18}$$

where $\mathbf{R}_{\hat{v}_{ab}}(\Delta t)$ represents the correlation matrix of wind components $\hat{v}_a$ and $\hat{v}_b$, that is

$$\mathbf{R}_{\hat{v}_{ab}}(\Delta t) = \mathbb{E}\left[\hat{v}_a(t)\hat{v}_b^T(t+\Delta t)\right]. \tag{19}$$

It is noticed that the expressions of $\mathbf{R}_{\hat{v}_{ab}}(\Delta t)$ can be obtained as a function of $\mathbf{R}_u(\Delta t)$, $\mathbf{R}_v(\Delta t)$ and $\mathbf{R}_w(\Delta t)$ no matter the degree of the polynomial transformation. Examples follow. In the frequency domain, the side-by-side Fourier transform of Eq. (18) gives

$$\mathbf{S}_{\hat{\boldsymbol{v}}}(\omega) = \begin{pmatrix} \mathbf{S}_{\hat{v}_{11}}(\omega) & \mathbf{S}_{\hat{v}_{12}}(\omega) & \cdots & \mathbf{S}_{\hat{v}_{1,\mathrm{NDEGW}}}(\omega) \\ \mathbf{S}_{\hat{v}_{21}}(\omega) & \mathbf{S}_{\hat{v}_{22}}(\omega) & & \mathbf{S}_{\hat{v}_{2,\mathrm{NDEGW}}}(\omega) \\ \vdots & & & \\ \mathbf{S}_{\hat{v}_{\mathrm{NDEGW},1}}(\omega) & & & \mathbf{S}_{\hat{v}_{\mathrm{NDEGW},\mathrm{NDEGW}}}(\omega) \end{pmatrix} \tag{20}$$

where, equivalently, all elements can be expressed as a function of $\mathbf{S}_u(\omega)$, $\mathbf{S}_v(\omega)$ and $\mathbf{S}_w(\omega)$.

Some of these large block-matrices in both Eqs. (18) and (20) can vanish or be neglected, especially if the correlation between elementary components of the turbulence are neglected.

As an example, Fig. 2-a shows the possible structure of $\mathbf{R}_{\hat{\boldsymbol{v}}}(\Delta t)$ and $\mathbf{S}_{\hat{\boldsymbol{v}}}(\omega)$ for $d = 2$, i.e. $\mathtt{NDEGW} = 9$. The diagonal elements represent $\mathbf{S}_u(\omega)$, $\mathbf{S}_v(\omega)$, $\cdots$, $\mathbf{S}_{vw}(\omega)$ at all nodes of the model. The colored boxes indicate where non-zero values can be found. Indeed, cross-correlation functions involving in total an odd number of powers of Gaussian processes vanish. Among all these possible non-zeros values, some might be neglected, especially in these two cases: (i) assuming the wind turbulence components are uncorrelated would discard all elements but the first six blocks of the main block-diagonal, (ii) assuming a small wind turbulence intensity would result in neglecting all elements but the first three blocks of the main block-diagonal.

Since not all wind components in Eq. (13) are Gaussian, higher statistical moments are required for a full probabilistic description of the loading. In particular, as soon as quadratic terms are considered ($d \geq 2$), the third rank statistical quantities known as the bicorrelation and the bispectrum need to be established. Thanks to the block matrix representation, the bicorrelation of wind components $\mathbf{R}_{\hat{\boldsymbol{v}}}(\Delta t_1, \Delta t_2)$ takes the form of a 3-D block-matrix composed of block-tensors $\mathbf{R}_{\hat{v}_{abc}}(\Delta t_1, \Delta t_2)$. An equivalent representation at third order consists in the bispectrum of the loading, which is formally obtained by the two-fold Fourier transform of the bicorrelation function. It is noted $\mathbf{B}_{\hat{\boldsymbol{v}}}(\omega_1, \omega_2)$ and is composed of the block-tensors $\mathbf{B}_{\hat{v}_{abc}}(\omega_1, \omega_2)$ corresponding to the bispectra of a given triplet of components a, b, c of wind loading components.

The format of $\mathbf{R}_{\hat{\boldsymbol{v}}}(\Delta t_1, \Delta t_2)$ and $\mathbf{B}_{\hat{\boldsymbol{v}}}(\omega_1, \omega_2)$ is depicted in Fig. 2-(b,c), for $d = 2$, where the larger shadowed blocks indicate the possible non-zero elements. It is interesting to notice that the first large block in Fig. 2-c, that is the only remaining block for $d = 1$, is exactly equal to zero. This translates the fact that the loading is Gaussian in case of linearized model. Then, if the cross-correlation between wind turbulence components $u(t)$, $v(t)$ and $w(t)$ is neglected, in the four large blocks with possible non-zero components, the only ones that remain are the block-tensors colored in red, yellow and blue in Fig. 2-b.

Higher order statistics could also be developed following the same approach. In the following illustrations, results are however limited to the third order analysis.

It is emphasized at this stage already that, as soon as $d \geq 2$, the size of matrices and tensors $\mathbf{R}_{\hat{\boldsymbol{v}}}(\Delta t)$, $\mathbf{S}_{\hat{\boldsymbol{v}}}(\omega)$ and $\mathbf{R}_{\hat{\boldsymbol{v}}}(\Delta t_1, \Delta t_2)$, $\mathbf{B}_{\hat{\boldsymbol{v}}}(\omega_1, \omega_2)$ is much larger than the size of the cross-correlation matrices (or cross-power spectral densities) which constitute the minimum independent information for this problem. To construct these full matrices before projecting them in a modal basis, as seen next, can therefore already be seen as an inefficient approach.

4. A quadratic wind loading model

In the previous Section, the general framework of the nonlinear wind loading model has been presented. It is now assumed that the block-matrix representation of the PSD and bispectrum of wind loads are known. In the following developments, only second and third orders will be treated so that these two pieces of information are sufficient. Also, a quadratic loading model is considered ($d = 2$) . The small turbulence intensity approximation is formulated and turbulence components are supposed to be uncorrelated so that : (i) only the first three blocks of the main block-diagonal in $\mathbf{R}_{\boldsymbol{v}}(\Delta t)$ and $\mathbf{S}_{\boldsymbol{v}}(\omega)$ remain, and (ii) only the colored blocks in Fig. 2-b are kept. To assume uncorrelated wind components is a simplification made for this particular example of wind loading; this prevents from having to choose among several existing cross-PSDs of turbulence components, but also to avoid the modeling of the spatial cross-coherence between various components of the wind turbulence. In any case, this simple choice is sufficient to illustrate the concepts developed in this paper. Interested readers could implement the same developments for the general nonlinear wind loading model introduced in Section 3.

Under these assumptions, the developments of the previous section to a quadratic wind loading model are specialized. The discussion is organized with respect to the modal wind loads, as introduced in Section 2. The wind force at all DOFs of a structural model, $\mathbf{f}(t)$, is given by Eq. (11), so that the modal force in mode m reads $p_m(t) = \boldsymbol{\phi}_m^T f(t)$ where $\boldsymbol{\phi}_m^T$ is the mth mode shape. Alternatively, it is also written

$$p_m(t) = \sum_{I=1}^{\mathrm{NN}} \sum_{a=1}^{\mathrm{NDEGW}} \alpha_{Ia}^{(m)} v_{Ia}(t) \tag{21}$$

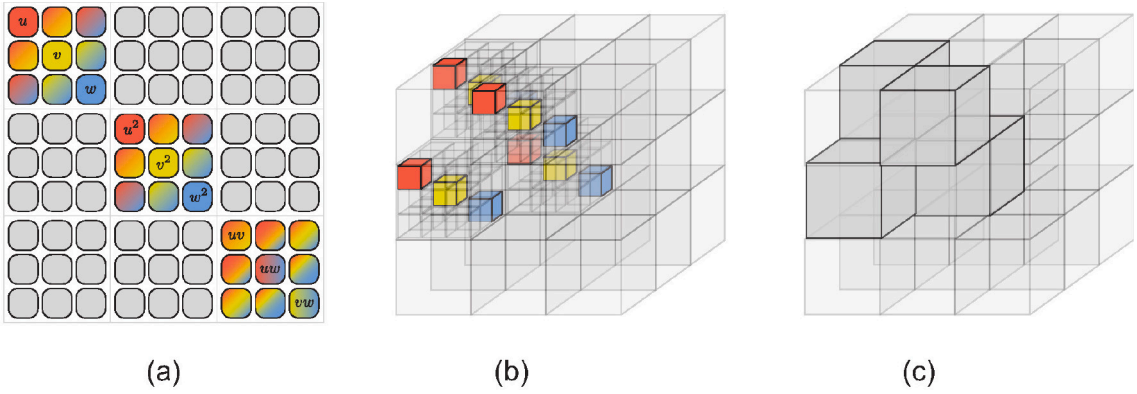

Fig. 2. (a) Block matrix representation of $\mathbf{R}_{\hat{b}}(\Delta t)$ and $\mathbf{S}_{\hat{b}}(\omega)$; (b–c) Block matrix representation of $\mathbf{R}_{\hat{b}}(\Delta t_1, \Delta t_2)$ and $\mathbf{B}_{\hat{b}}(\omega_1, \omega_2)$.

where $\alpha_{Ia}^{(m)} = \boldsymbol{\phi}_m^T \mathbf{a}_{Ia}$ is a modal loading coefficient combining the influence of the wind loads in mode m resulting from loads at all degrees-of-freedom and from the wind load at the aerodynamic node I. This formulation takes the same linear combination as for wind load at physical degrees-of-freedom, see Eq. (12).

4.1. Second order

At second order, statistical information is given either by the Auto-correlation function in the time domain, either by the Power Spectral Density (PSD) function in the frequency domain. In time domain, the cross-correlation function of modal forces in modes m and n is obtained by considering Eq. (21), which gives

$$R_{p_{mn}}(\Delta t) = \mathbb{E}\left[p_m(t) p_n(t+\Delta t)\right] = \sum_{a=1}^{\text{NDEGW}} \sum_{b=1}^{\text{NDEGW}} R_{p_{mn}}^{(ab)}(\Delta t) \tag{22}$$

where $R_{p_{mn}}^{(ab)}(\Delta t) = \sum_{I=1}^{\text{NN}} \sum_{J=1}^{\text{NN}} \alpha_{Ia}^{(m)} \alpha_{Jb}^{(n)} \mathbb{E}\left[\upsilon_{Ia}(t) \upsilon_{Jb}(t+\Delta t)\right]$ quantifies how the cross-correlation between wind components a and b contributes to the total amount of correlation between the two considered modal forces. Taking the Fourier Transform of Eq. (22), we have

$$S_{p_{mn}}(\omega) = \sum_{a=1}^{\text{NDEGW}} \sum_{b=1}^{\text{NDEGW}} S_{p_{mn}}^{(ab)}(\omega) \tag{23}$$

in which $S_{p_{mn}}^{(ab)}(\omega) = \sum_{I=1}^{\text{NN}} \sum_{J=1}^{\text{NN}} \alpha_{Ia}^{(m)} \alpha_{Jb}^{(n)} S_{\upsilon_{Ia}\upsilon_{Jb}}(\omega)$ represents the contribution of the cross-PSD between wind components a and b to the cross-PSD of wind loads in modes m and n.

Under the assumptions considered in this Section, the only components of the wind loading that are necessary are $(a,b) \in \{(1,1),(2,2),(3,3)\}$, so that, in a general fashion,

$$S_{p_{mn}}^{(ab)}(\omega) = \sum_{I=1}^{\text{NN}} \sum_{J=1}^{\text{NN}} \alpha_{Ia}^{(m)} \alpha_{Jb}^{(n)} S_{\upsilon_{Ia}\upsilon_{Jb}}(\omega). \tag{24}$$

For example, considering $a = b = 1$, $\upsilon_{Ia} = u_I$ and $\upsilon_{Jb} = u_J$ respectively correspond to the longitudinal component of turbulence at nodes I and J, so that $\mathbb{E}\left[\upsilon_{Ia}(t)\upsilon_{Jb}(t+\Delta t)\right] = R_{u_I u_J}(\Delta t)$, but also

$$S_{p_{mn}}^{(11)}(\omega) = \sum_{I=1}^{\text{NN}} \sum_{J=1}^{\text{NN}} \alpha_{I1}^{(m)} \alpha_{J1}^{(n)} S_{u_I u_J}(\omega) \tag{25}$$

where the cross-PSD of the longitudinal turbulence components are classically expressed as

$$S_{u_I u_J}(\omega) = \Gamma_{IJ}(\omega) \sqrt{S_{u_I}(\omega) S_{u_J}(\omega)} \tag{26}$$

and $\Gamma_{IJ}(\omega)$ is the spatial coherence function of the wind turbulent component $u(t)$, evaluated at the two nodes I and J. Same developments apply for $a = b = 2$ and $a = b = 3$, noticing however that the coherence function might be adapted for other elementary turbulence components.

4.2. Third order

At third order, in time domain the bicovariance function for stationary processes is defined as a function of two time lags with respect to the reference process. In particular, the bicovariance function of modal forces m, n and o reads

$$R_{p_{mno}}(\tau_1, \tau_2) = \mathbb{E}\left[p_m(t) p_n(t+\tau_1) p_o(t+\tau_2)\right]. \tag{27}$$

Similarly as in Eq. (22),

$$R_{p_{mno}}(\tau_1, \tau_2) = \sum_{a=1}^{\text{NDEGW}} \sum_{b=1}^{\text{NDEGW}} \sum_{c=1}^{\text{NDEGW}} R_{p_{mno}}^{(abc)}(\tau_1, \tau_2) \tag{28}$$

where $R_{p_{mno}}^{(abc)}(\tau_1, \tau_2) = \sum_{I=1}^{\text{NN}} \sum_{J=1}^{\text{NN}} \sum_{K=1}^{\text{NN}} \alpha_{Ia}^{(m)} \alpha_{Jb}^{(n)} \alpha_{Kc}^{(o)} \mathbb{E}\left[\upsilon_{Ia}(t) \upsilon_{Jb}(t+\tau_1) \upsilon_{Kc}(t+\tau_2)\right]$ represents the contribution of the bicovariance function of elementary wind components a, b and c to the bicovariance of wind loads in modes m, n and o. Application of the double Fourier Transform to Eq. (28) gives the bispectrum of modal loads

$$B_{p_{mno}}(\omega_1, \omega_2) = \sum_{a=1}^{\text{NDEGW}} \sum_{b=1}^{\text{NDEGW}} \sum_{c=1}^{\text{NDEGW}} B_{p_{mno}}^{(abc)}(\omega_1, \omega_2) \tag{29}$$

where $B_{p_{mno}}^{(abc)}(\omega_1, \omega_2)$ represents the contribution of the triplet of wind components (a,b,c) to the total bispectrum. This contribution can be expressed as a function of the power spectral density of the turbulence components as discussed earlier. Under the assumptions made in this Section, only some triplets (a,b,c) identified in the grayed boxes in Fig. 2-c do contribute to the bispectrum of wind loads. For instance, for $a = 4$ and $b = c = 1$ (component involving $u_I^2(t)$, $u_J(t)$ and $u_K(t)$ in Eq. (16)), the contribution $R_{p_{mno}}^{(abc)}(\tau_1, \tau_2)$ to the autocorrelation becomes

$$R_{p_{mno}}^{(411)}(\tau_1, \tau_2) = \sum_{I=1}^{\text{NN}} \sum_{J=1}^{\text{NN}} \sum_{K=1}^{\text{NN}} \alpha_{I4}^{(m)} \alpha_{J1}^{(n)} \alpha_{K1}^{(o)} \mathbb{E}\left[u_I^2(t) u_J(t+\tau_1) u_K(t+\tau_2)\right]. \tag{30}$$

It can be proved that, after developing the expectation operator, Eq. (30) becomes

$$R_{p_{mno}}^{(411)}(\tau_1, \tau_2) = \sum_{I=1}^{\text{NN}} \sum_{J=1}^{\text{NN}} \sum_{K=1}^{\text{NN}} \alpha_{I4}^{(m)} \alpha_{J1}^{(n)} \alpha_{K1}^{(o)} \times \left(R_{u_I u_J}(\tau_1) R_{u_I u_K}(\tau_2) + \sigma_u^2 R_{u_J u_K}(\tau_2 - \tau_1)\right) \tag{31}$$

In the frequency domain, the important contribution of the triplet $(4,1,1) \equiv (u^2, u, u)$ to the total cross-bispectrum of the modal force (m,n,o) is

$$B_{p_{mno}}^{(411)}(\omega_1, \omega_2) = \sum_{I=1}^{\text{NN}} \sum_{J=1}^{\text{NN}} \sum_{K=1}^{\text{NN}} \alpha_{I4}^{(m)} \alpha_{J1}^{(n)} \alpha_{K1}^{(o)} S_{u_I u_J}(\omega_1) S_{u_I u_K}(\omega_2) \tag{32}$$

since the term depending on the single autocorrelation function $R_{u_J u_K}(\tau_2 - \tau_1)$ does not contribute to the cumulant (it actually provides a Dirac

delta function in the frequency domain). Other triplets, expressed as similar combinations of $u_I^2(t)$, $u_J(t)$ and $u_K(t)$ (one squared and two original values) can be derived in the same way. In the following example, the mixed contributions coming from mixed combinations of $u(t)$, $v(t)$ and $w(t)$ at different nodes are disregarded. Similar formulations can be retrieved for all the triplets (a, b, c) of wind components contributing, under the considered assumptions, to the construction of the full 3D matrix of bispectrum of modal forces. They are not shown in detail. However, they are obtained with the same approach as shown above for deriving Eq. (32).

5. Double modal transformation at second and third statistical orders

Once the PSD matrix and the tensor of bispectra of modal wind loads are determined, the analysis can follow the general steps described in Section 2. However, it is computationally demanding to construct such a huge amount of information, based on the single PSD matrices of wind turbulence components.

5.1. Second order

For this reason Carassale et al. have suggested to approach the structural analysis by means of a double modal transformation (Carassale et al., 2001). This approach is summarized here, then extended at third order in the context of the bispectral analysis.

Under a very general point of view, $S_{u_I u_J}(\omega)$ might be seen as a single element of the large Cross Power Spectral Density Matrix (CPSDM) (Carassale et al., 2001) of wind turbulence at the (aerodynamic) nodes of the model. For the longitudinal component $u(t)$, it is written $\mathbf{S}_u(\omega)$. The spectral decomposition of $\mathbf{S}_u(\omega)$, obtained by solving

$$\left[\mathbf{S}_u(\omega) - \lambda_p(\omega)\mathbf{I}\right]\boldsymbol{\psi}_p(\omega) = \mathbf{0} \qquad (p = 1, \dots, \mathtt{NN}) \tag{33}$$

reads

$$\mathbf{S}_u(\omega) = \boldsymbol{\Psi}(\omega)\ \boldsymbol{\Lambda}(\omega)\ \boldsymbol{\Psi}^T(\omega) \tag{34}$$

where $\boldsymbol{\Lambda}(\omega)$ and $\boldsymbol{\Psi}(\omega)$ are the (frequency dependent) diagonal eigenvalues and eigenvector matrices respectively, resulting from the eigenproblem in Eq. (33). It is assumed that the eigenvalues are sorted in descending order in $\boldsymbol{\Lambda}(\omega)$. All of them are positive because of the positivity of the CPSDM $\mathbf{S}_u(\omega)$. Keeping only the first $\mathtt{N_p} \ll \mathtt{NN}$ modes with significant eigenvalues, Eq. (34) can be rewritten as

$$S_{u_I u_J}(\omega) = \sum_{p=1}^{\mathtt{N_p}} \psi_{Ip}(\omega)\lambda_p(\omega)\psi_{Jp}(\omega). \tag{35}$$

Injecting Eq. (35) in Eq. (25):

$$S^{(11)}_{p_{mn}}(\omega) = \sum_{p=1}^{\mathtt{N_p}}\sum_{I=1}^{\mathtt{NN}}\sum_{J=1}^{\mathtt{NN}} \alpha^{(m)}_{I1}\alpha^{(n)}_{J1}\psi_{Ip}(\omega)\lambda_p(\omega)\psi_{Jp}(\omega) \tag{36}$$

which could seem to be more involved but, swapping summations and writing more generally, we have

$$S^{(ab)}_{p_{mn}}(\omega) = \sum_{p=1}^{\mathtt{N_p}} \zeta^{(m)}_{pa}(\omega)\,\lambda_p(\omega)\zeta^{(n)}_{pb}(\omega) \tag{37}$$

where

$$\zeta^{(m)}_{pa}(\omega) = \sum_{I=1}^{\mathtt{NN}} \alpha^{(m)}_{Ia}\psi_{Ip}(\omega). \tag{38}$$

The double sum over the number NN of loaded nodes as in Eq. (23) has dropped in place of a single sum over the $\mathtt{N_p} \ll \mathtt{NN}$ kept modes of the spectral decomposition of $u(t)$. Eq. (37) is definitely much more efficient to implement than Eq. (25). It just requires the prior computation and storage of $\zeta^{(m)}_{pa}(\omega)$ for $a \in \{1, 2, 3\}$, for the three wind turbulence components only. Again, similar expressions are obtained for the other components of wind turbulence.

5.2. Third order

At second order, application of dimensionality reduction techniques to stochastic analysis of structures in wind engineering was already tackled (Carassale et al., 2001) and claimed to be very efficient. The applied concepts are the same as in Eq. (36), but their application to third order statistics shows some substantial differences. The most significant is the dependence to not just one but two frequencies, ω_1 and ω_2.

Following the concepts explained in detail for Eqs. (34) and (35), it is possible to express the two PSDs of wind turbulence as a sum of some principal components

$$\begin{aligned} S_{u_I u_J}(\omega_1) &= \sum_{p=1}^{\mathtt{N_p}} \psi_{Ip}(\omega_1)\lambda_p(\omega_1)\psi_{Jp}(\omega_1) \quad ; \\ S_{u_I u_K}(\omega_2) &= \sum_{q=1}^{\mathtt{N_q}} \psi_{Iq}(\omega_2)\lambda_q(\omega_2)\psi_{Kq}(\omega_2). \end{aligned} \tag{39}$$

Injecting Eq. (39) into Eq. (32) yields

$$B^{(411)}_{p_{mno}}(\omega_1, \omega_2) = \sum_{p=1}^{\mathtt{N_p}}\sum_{q=1}^{\mathtt{N_q}} \zeta^{(n)}_{p1}(\omega_1)\,\zeta^{(o)}_{q1}(\omega_2)\,\chi^{(m)}_{pq4}(\omega_1, \omega_2)\,\lambda_p(\omega_1)\lambda_q(\omega_2) \tag{40}$$

where

$$\chi^{(m)}_{pqa}(\omega_1, \omega_2) = \sum_{I=1}^{\mathtt{NN}} \alpha^{(m)}_{Ia}\psi_{Ip}(\omega_1)\,\psi_{Iq}(\omega_2). \tag{41}$$

Another substantial difference is in the term $\chi^{(m)}_{pqa}(\omega_1, \omega_2)$ appearing in Eq. (40) which couples the dependence on the two independent variables ω_1 and ω_2. There is no doubt that the double summation over loading modes in Eq. (40) is much more efficient than the three-fold summation over the total number of aerodynamic nodes in Eq. (32).

The computational cost to estimate each $\zeta^{(m)}_{pa}(\omega)$ requires a loop on all aerodynamic nodes, and this operation needs to be done for combinations (m, p, a), i.e. $\mathtt{NM} \times \mathtt{N_p} \times \mathtt{NDEGW}$. The computational cost to estimate each $\chi^{(m)}_{pqa}(\omega_1, \omega_2)$ also requires a loop on all nodes, and this operation needs to be done for combinations (m, p, q, a), i.e. $\mathtt{NM} \times \mathtt{N_p} \times \mathtt{N_q} \times \mathtt{NDEGW}$.

6. Recombination of modal responses

At the beginning of Section 2, equations of motions have been projected in the modal basis. This brings many advantages to the analysis, especially the reduction of the size of the problem. After a structural analysis in the modal basis, the structural responses in the Euclidian space are obtained by recombination of modal responses, using again $\mathbf{x}(t) = \boldsymbol{\Phi}\mathbf{q}(t)$. In the context of a stochastic analysis, this is done in terms of statistical moments.

There are different ways for recombining modal responses in order to recover structural ones. At second order, this is done through the Complete Quadratic Combination (CQC) or the known Square Root of Sum of the Squares (SRSS)

$$m^{CQC}_{2,x_i} = \sum_{m=1}^{\mathtt{NM}}\sum_{n=1}^{\mathtt{NM}} \phi_{im}\phi_{in}m_{2,q_{mn}} \tag{42}$$

$$m^{SRSS}_{2,x_i} = \sum_{m=1}^{\mathtt{NM}} \phi^2_{im}m_{2,q_m} \tag{43}$$

the second one being a particular case of the former when correlation between modal responses can be neglected.

At third order, the same combination principles can be extended to the so-called Cubic Root of Sum of the Cubes (CRSC) or the Complete Cubic Combination (CCC), see Denoël et al. (2023),

$$m^{CCC}_{3,x_i} = \sum_{m=1}^{\mathtt{NM}}\sum_{n=1}^{\mathtt{NM}}\sum_{o=1}^{\mathtt{NM}} \phi_{im}\phi_{in}\phi_{io}\ m_{3,q_{mno}} \tag{44}$$

$$m_{3,x_i}^{CRSC} = \sum_{m=1}^{NM} \phi_{im}^3 \, m_{3,q_m} \tag{45}$$

Finally, Eqs. (42) to (45) are used for the estimation of extreme values (Kwon and Kareem, 2009) of structural responses (e.g. nodal displacements or internal forces). Denoting the average of a structural response as $\overline{x}_i$ (obtained with a separate static analysis), the standard deviation as $\sigma_{x_i} = \sqrt{m_{2,x_i}}$, and the peak factor as g_{G_i}, $g_{nG_i^+}$ and $g_{nG_i^-}$ (depending on the approach used to determine it), the extreme values to be used for a design are given by

$$\overline{x}_{G_i} = \overline{x}_i + g_{G_i}\sigma_{x_i} \tag{46}$$

$$\overline{x}_{nG_i^+} = \overline{x}_i + g_{nG_i^+}\sigma_{x,i} \quad ; \quad \overline{x}_{nG_i^-} = \overline{x}_i - g_{nG_i^-}\sigma_{x,i} \tag{47}$$

They correspond to the Gaussian extreme value Eq. (46), and to the positive (resp. negative) non-Gaussian extreme values Eq. (47). While the peak factor g_{G_i} is determined by means of Rice's formula assuming independent crossings, the non Gaussian peak factors $g_{nG_i^+}$ and $g_{nG_i^-}$ depend on the skewness (hence m_{3,x_i}). In the following illustrations, the Kareem-Zhao formula (Gurley et al., 1997) has been used, together with the assumption that the excess coefficient corresponds to the monotone limit; this assumption is similar to what has been used in Denoël et al. (2023) where a very good agreement with Monte Carlo simulations has been shown.

7. Overview of the algorithmic arrangement

Recalling what has been stated at the end of Section 2, there are two major challenges when it comes to higher order spectral analysis: (i) the optimal establishment of spectra of modal solicitations, (ii) the optimal but accurate integration of the resulting spectra of the structural response, needed for estimating extremes values according to Eqs. (46) or (47). Indeed, projection of the spectra of loading in the modal basis is definitely the most expensive operation. In order to tackle this computational burden, we employed both mathematical and numerical tools. Indeed, mathematical side has been extensively discussed in previous sections, by extending the double modal transformation to bispectral analysis. Alongside, we employed a novel algorithmic structure in order to maximize efficiency, which aims at minimizing CPU time while at the same time minimizing estimation errors. We sought a balance between two extreme (unacceptable) solutions corresponding to (i) very fast but inaccurate or (ii) very accurate but extremely slow computations. Indeed, both scenarios must be avoided. The main concept of the algorithm lies on a 2-stage discretization of the 2D frequency space. The first stage consists in a first optimal discretization of the frequency space aiming at representing the bispectrum of modal loads. This task is achieved by a dense sampling in the neighborhood of the origin $(\omega_1, \omega_2) = (0, 0)$ where the bispectrum of loading has large gradients. In the second stage, the bispectrum of modal responses need to be determined and integrated. Because of large resonance peaks in the kernel, many integration points are required in the neighborhood of the resonance peaks. In those areas, the bispectrum of the loading is typically smooth and can be interpolated over the looser mesh utilized in the first stage.

In each of the two stages, the sampling method is systematic and not adaptive; indeed the regions where sampling is required are easily identifiable in advance : in the low frequency zone (so called quasi-static basin) for the loading, then in the neighborhood of resonance peaks and crests in the second stage (Denoël, 2011). This approach has been found superior to the adaptive integration scheme which would have to face three major issues: (i) storage, since one should keep track of all the 2D frequency pairs (ω_1, ω_2) for which a discretization point is added due to the refinement process, which could not be retrieved otherwise; (ii) efficiency, in terms of computational CPU time, since a gradient condition should be checked for each added point, (iii) complexity, at the level of determining the influence area of each discretization point, (ω_1, ω_2) for the integration process.

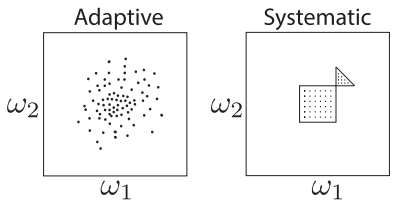

Fig. 3. Discretization of the 2D frequency space. (a) adaptive, (b) systematic/zoned.

In order to overcome these possible issues, we introduced in the systemic sampling the concept of "zone" as being as sub-part of the domain of integration. Specifically, we discretize the domain into non-overlapping and complementary sub-spaces (e.g. zones) where each of them has a regular, internal discretization. The mesh density varies from zone to zone. In the case of bispectral analysis, these elemental zones reduce to rectangles and triangles patching the 2D frequency plane. Fig. 3 shows a simple example explaining graphically both these concepts. In the following illustrations, different colors will be used for the different zones so that they can be easily identified.

The other important point is that a zone, based on its definition, can be placed anywhere in the domain of integration. Moreover, following the 2-stage meshing approach described earlier, the use of zones allows the definition of the first discretization even before the actual computation starts. For instance, modal loads could be treated independently of knowing natural frequencies. Once this is done, each zone is treated independently, and the POD decomposition of the wind field is extensively exploited in order to project the bispectrum of aerodynamic loads in the modal basis. Then, once this first discretization is established, a finer discretization is built on top of it, where structural response statistical information is consequently computed. Another clear advantage of using the "zoned" approach relies on the fact that interpolation can be done independently for each zone, based on its internal discretization, in the manner of an object-oriented approach. This eases the dispatching of the computational tasks to several units.

In summary, this novel 2-stage integration scheme addresses the aforementioned issues:

- storage, since now only very few information needs to be stored in order to uniquely identify and characterize an elemental zone. Then, in a post-processing phase, the actual internal discretization can be easily and efficiently reconstructed, without the actual need to store it entirely;
- efficiency, since now each independent zone has its own, regular internal discretization. This can then be freely chosen and predetermined based on some desired constraints, depending on which actual part of the domain the same zone is going to cover. Once defined, no need to perform any convergence verification;
- complexity, since again, having each zone its own independent internal discretization, each point will have an influence area which is easily known at the time of the zone definition.

Last but not least, the proposed methodology is applicable to more general cases, included those where assumptions at the base of a Multiple Timescale Spectral Analysis (MTSA) are not strictly met, e.g. loading and structural time scales which are almost comparable (Denoël, 2015). It is also possible to develop the same concept at higher orders.

8. Application to a real example

8.1. Description of the case study

In order to test and prove the proposed methodology, we applied it to a fairly real, yet academic, example. A choice has been made among 18 bridge decks studied in Flamand and Denoël (2011), where

Fig. 4. Photo of the Quetzalapa Bridge, Mexico.
Source: http://www.highestbridges.com/wiki/index.php?title=Quetzalapa_Bridge.

Table 1
Natural frequencies, damping ratios and modal masses for the first four vibration modes.

Mode [–]	Natural frequency [Hz]	Structural [%]	Aero [%]	Modal mass [to.]
1	0.952	3%	0.45%	26 031
2	1.452	3%	0.85%	28 973
3	1.788	3%	0.48%	38 343
4	3.640	3%	0.07%	22 075

Table 2
Summary of important wind turbulence properties.

Turbulence	Lengthscale [m]	Std [m/s]	Coherence coeff. [–]
$u(t)$	250	6.5	12
$w(t)$	200	5.24	12

the authors compare and classify according to the bridge topologies the wind force coefficients measured for 18 different cross-sections. The choice has fallen on the twin-girder Quetzalapa Bridge, built in Mexico in 1993 on the famous Mexico City-Acapulco highway, after the other famous Mezcala Bridge. It is a two H-tower cable-stayed bridge, with main span of 213 m, with maximum height of 110 m (see Fig. 4).

Top part of Fig. 5-a shows the simplified structural scheme. A 3-span simply supported bridge model has been assumed, with main span of 150 m, lateral spans of 120 m each. Each span has been modeled with 20 beam elements of equal length. The value of the bending stiffness is chosen as $EI = 2.785 \cdot 10^{13}$ Nm^2 and the mass per unit length is equal to 130 000 kg/m. The deck width is 29.50 m. On the bottom part of Fig. 5, the first 4 vibration modes, in the vertical direction, are shown. In total, the model comprises 366 DOFs and seven modes are used in the bispectral analysis. A damping ratio of 3% has been imposed to all vibration modes. In addition to that, the aerodynamic damping has also been computed with a quasi-steady analysis, and taken into account. Table 1 lists the damping ratios for the first 4 vibration modes as well as natural frequencies and modal masses.

Only the left-most span has been assumed loaded by the turbulent wind flow. Indeed, in deep valleys, the wind flow attacking a bridge deck might be uneven and sheltering effects might result in very unequal loads on the different parts of the deck. This choice has also been made in this context for maximizing the asymmetry in the loading resulting therefore in a critical design situation. Besides, with a wind load distributed along a shorter area, the modal loads and therefore the modal responses too, tend to be more non Gaussian.

Fig. 5-b shows the variation of drag and lift wind coefficients measured in the wind tunnel tests performed on the bridge model, tested at the CSTB, Nantes (Flamand and Denoël, 2011), as well as C_Z, the resultant along the vertical axis in the local element reference system of the drag and lift coefficients, as depicted schematically in Fig. 5-b. This example has been chosen for the nonlinear nature of the vertical coefficient with respect to the wind angle of attack. In order to simplify the aerodynamic modeling, the vertical force coefficient has been approximated by a quadratic function which results in a non-Gaussian wind loading.

More specifically, the illustration focuses on the vertical vibrations of the bridge resulting from this vertical wind load (per unit length), which is defined as:

$$F_Z(t) = \frac{1}{2}\rho C_Z\left[\beta\left(t\right)\right] V^2\left(t\right) B \tag{48}$$

where C_Z is the vertical wind force coefficient, measured in the wind tunnel. In a quasi-steady approach, Eq. (48) translates the influence of the wind turbulence into forces applied to the structure, with which engineers can perform usual static/dynamic analyses. The nonlinearity is hidden behind two factors in Eq. (48): (i) V^2 which is the square of the norm of the (instantaneous) wind speed vector

$$V^2 = \overline{U}^2 + 2\overline{U}u + u^2 + v^2 + w^2 \tag{49}$$

and (ii) $C_Z = C_Z\left[\beta(t)\right]$ the vertical wind force coefficient, which is a function of $\beta(t)$ the instantaneous incidence of the wind speed, see Fig. 5-b. In spite of existing more general 3-D models of wind loads (da Costa et al., 2022), lacking modeling information, we assume here a 2-D model where the wind incidence fluctuates around its mean value $\beta(t) = \overline{\beta} + \Delta\beta(t)$, where $\Delta\beta(t)$ is the instantaneous fluctuation from mean incidence angle at time t. Assuming this deviation to be small, the wind force coefficient C_Z is expressed via a Taylor series expansion around the mean incidence angle $\overline{\beta} = -1°$:

$$C_Z(\beta(t)) = C_Z(\overline{\beta}) + \partial_\beta C_Z(\overline{\beta})\Delta\beta(t) + \frac{1}{2}\partial_\beta^2 C_Z(\overline{\beta})\Delta\beta^2(t) + \ldots \tag{50}$$

so that $C_Z(\overline{\beta}) = -0.35$, $\partial_\beta C_Z(\overline{\beta}) = 8.5$ and $\partial_\beta^2 C_Z(\overline{\beta}) = 72.5$, see quadratic approximation in Fig. 5-c, and

$$\Delta\beta(t) = \arctan\left(\frac{w(t) - \dot{h}(t)}{\overline{U} + u(t)}\right) \tag{51}$$

in a simplified scenario where the along-wind structural motion has not been taken into account. Since vertical motion only is considered in this example, the relative angle of attack is computed by subtracting the heaving velocity $\dot{h}(t)$ to the vertical turbulence component.

Substitution of (49)–(51) into Eq. (48), and series expansion for small u, w and $\dot{h}$ yields

$$\begin{aligned} F_Z(t) = \overline{F_Z} &+ \frac{1}{2}\rho B\overline{U}\left(2C_Z\left(\overline{\beta}\right)u + \partial_\beta C_Z(\overline{\beta})\left(w - \dot{h}\right)\right) \\ &+ \frac{1}{2}\rho B\overline{U}\left(C_Z\left(\overline{\beta}\right)\left(u^2 + w^2\right) + \partial_\beta C_Z(\overline{\beta})u\left(w - \dot{h}\right)\right. \\ &\left. + \frac{1}{2}\partial_\beta^2 C_Z(\overline{\beta})\left(w - \dot{h}\right)^2\right) \end{aligned} \tag{52}$$

where $\overline{F_Z} = \frac{1}{2}\rho C_Z(\overline{\beta})\overline{U}^2 B$ is the average aerodynamic load (treated in a separate static analysis), and the linear and quadratic loading terms are readily identified. In this expression, the argument (t) has been removed to simplify the notation and the transverse component of the wind $v(t)$, parallel to the bridge axis, has also been neglected. By keeping or discarding the second line in Eq. (52), the quadratic loading terms are kept or discarded. Table 2 lists all the relevant data regarding the wind turbulence, having a mean wind speed of $\overline{U} = 38$ [m/s].

Concerning the spectral and bispectral analyses, several variants are considered. First, in order to evaluate the importance of the spatial coherence of wind turbulence (and consequently buffeting loads), a variant of the original problem with coherence coefficients for u and w tending towards infinity is simulated. This variant is labeled "D-" in the following Figures, to highlight the fact that the CPSD matrices of turbulence components are *D*iagonal in that case, i.e. POD modes already correspond to the physical loads. This variant is not really physical but is a simple approach to reveal size effects of the structure. Second, for each considered buffeting loading, either full or diagonal CPSD matrices, modal responses are computed and recombined with the two recombination techniques presented in Section 6, namely an SRSS/CRSC or a CQC/CCC approach.

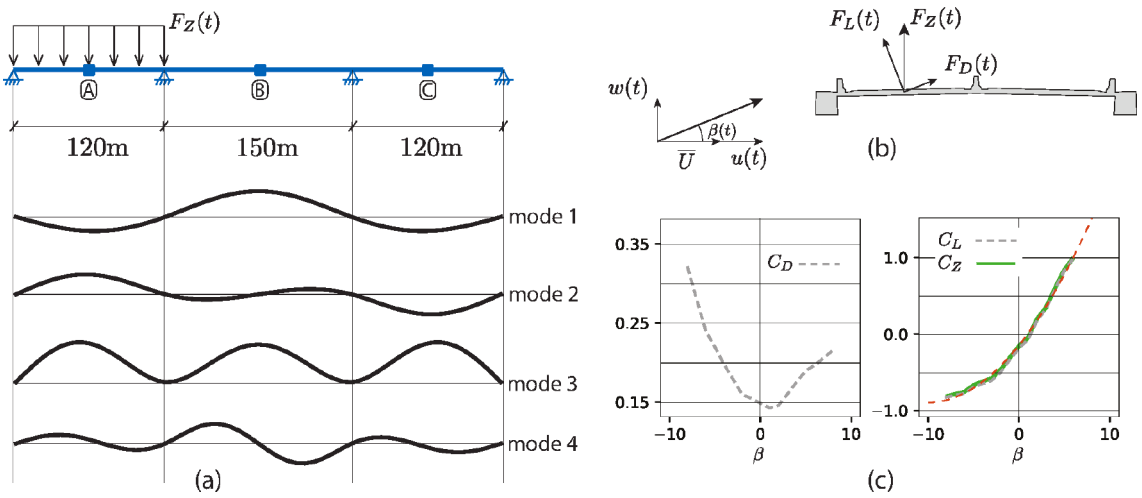

Fig. 5. (a) Sketch of the studied structure and mode shapes, (b) conventions for aerodynamic loads, (c) considered aerodynamic coefficients.

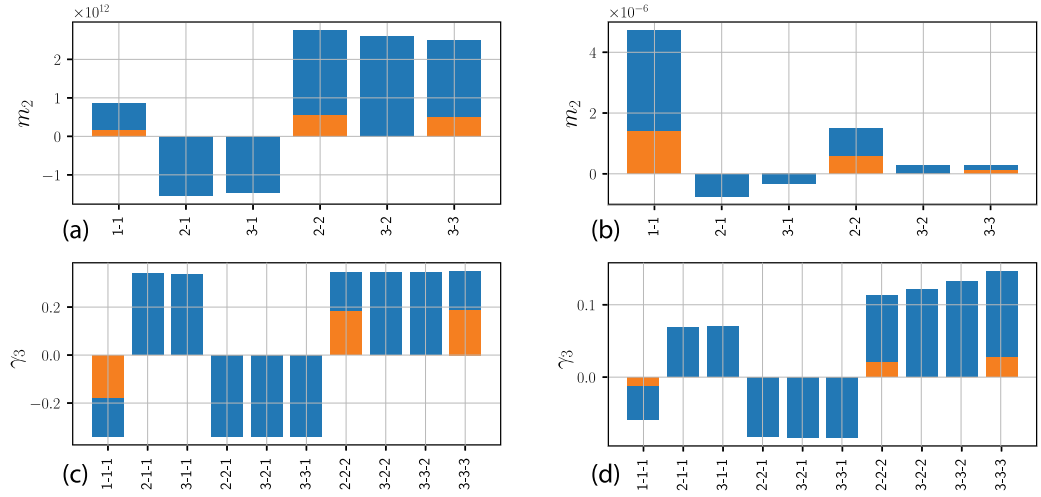

Fig. 6. 2nd and 3rd order moments of modal forces and modal responses: (a–c) modal loads, (b–d) modal responses. Colors refer to the approximation in spatial coherence: blue = full CPSD matrix of turbulence components, orange = diagonal CPSD matrix of turbulence components (variant D).

8.2. Results of the bispectral analysis - influence of modeling options

Fig. 6 shows the 2nd and 3rd order moments (in terms of variance/covariance and skewness) of modal loads and modal responses, for the modes 1, 2, and 3, which respond the most to the considered loading. Fig. 6-(a, b) refer to covariances, while Fig. 6-(c, d) show third order moments translated in terms of skewness coefficients. Also, 6-(a, c) refer to modal loads while 6-(b, d) to modal responses. Bars in blue refer to the moments obtained with the full CPSD matrix of turbulence components, while orange bars correspond to the diagonal version (variant D). In the latter case, only diagonal elements of the covariance matrix and of the triple correlation tensor are computed since only the SRSS/CRSC combination is considered in that case.

It is observed that the diagonal elements of the covariance matrix and of the triple correlation tensor of modal loads are much smaller in variant D than in the original problem with the actual spatial coherence. At second order, this translates the fact that the many aerodynamic forces distributed along the bridge deck possess a certain coherence in space and little compensations are observed during projection in the modal basis. However, for uncorrelated wind loads at the different nodes of the model, such compensations dominate and the projected wind field is consequently much smaller. At third order, the same reasoning holds and explains why the third statistical moment also drops in variant D. In fact, it drops more proportionally than the second moment since the skewness coefficient ($\gamma_3 = m_3/m_2^{3/2}$) also drops in the same variant. This is explained by the central limit theorem stating that a linear combination of independent processes tends to become Gaussian as the number of independent processes tends to infinity. In variant D, the applied loads are fully independent (uncorrelated), while there exists some partial correlation in the original problem. It is therefore expected that the non-Gaussianity of the combination (i.e. of the modal load) is smaller in variant D.

Fig. 6 also shows that the skewness of modal responses are smaller than the skewness of modal loads. This is also a consequence of the central limit theorem. Indeed, if the response was quasi-static (fully background), the modal response at a given time would be dependent on the modal load at the same time and there would be the same non-Gaussianity, i.e. the same skewness, in the response and in the loading. As the dynamic (resonant) part of the response becomes more important, for instance in case of small damping, the response at a given time is obtained as a convolution of loads applied at many more instants in the past. This means that there are more terms affecting the response at a given time and the response tends to be more Gaussian, i.e. symmetric in distribution. In the limit case of a fully resonant response, the skewness tends to zero and the response process is statistically symmetric.

Examples of power spectral densities of the structural displacements are three selected points of the bridge are shown in Fig. 7. The location

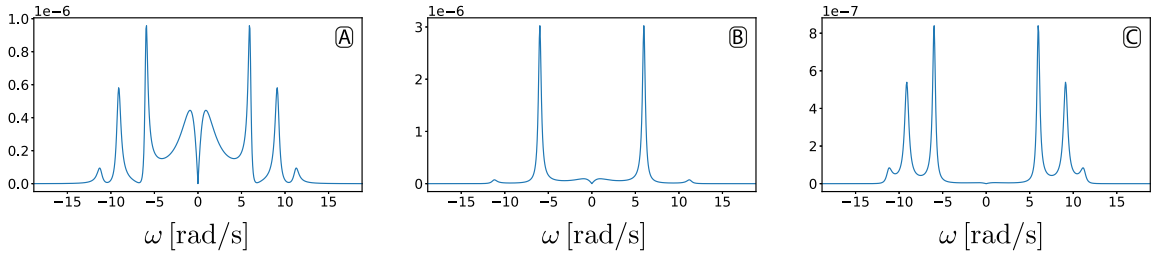

Fig. 7. Response PSDs, Ff-, at selected nodes, (A) node 10; (B) node 31; (C) node 52.

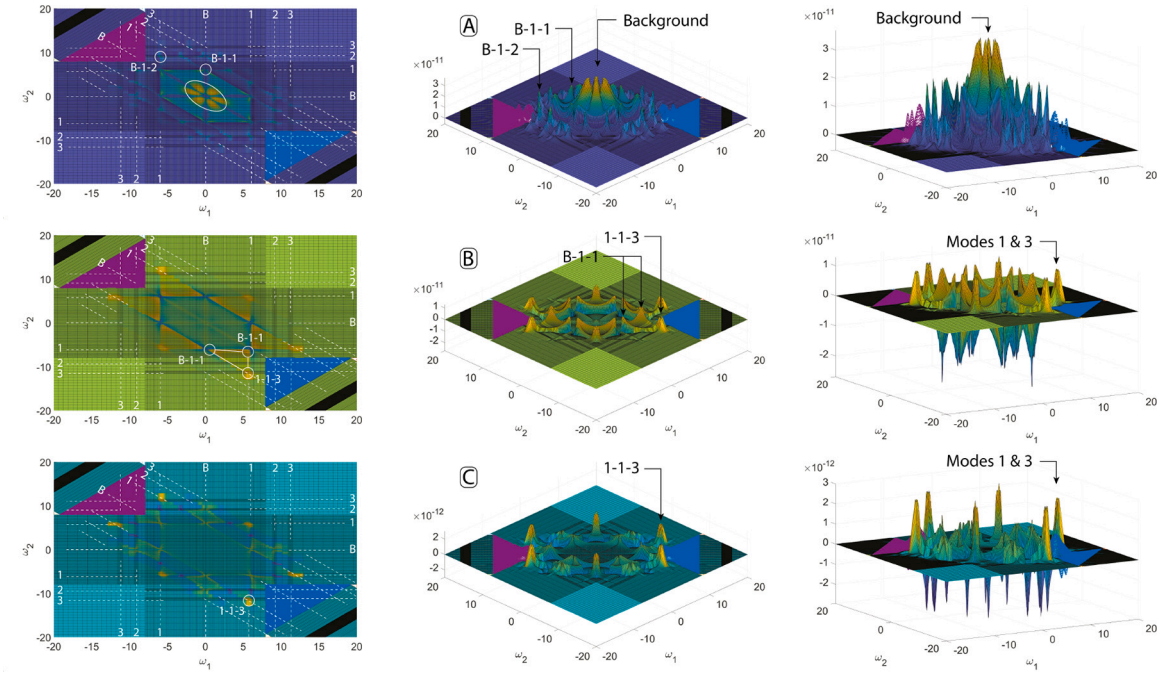

Fig. 8. Response bispectrum, Ff-, at selected nodes, (A) node 10; (B) node 31; (C) node 52.

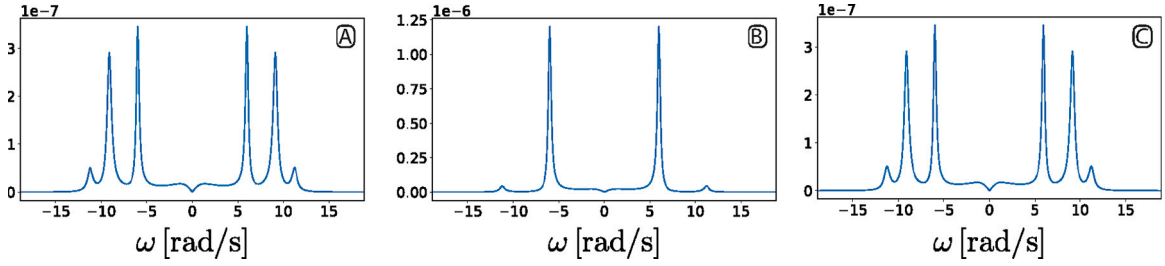

Fig. 9. Response PSDs, variant D-, at selected nodes, (A) node 10; (B) node 31; (C) node 52.

of points A, B and C correspond to the midspans, see Fig. 5-a. While the response at node A exhibits a significant background contribution, the responses at nodes B and C are mostly resonant. Similarly, the bispectrum of nodal displacements at nodes A, B and C are reported in Fig. 8, showing a significant background for node A and resonant responses in modes 1 and 3 for nodes B and C. These power spectral densities and bispectra are obtained with the full CPSD matrix of wind turbulence and with the complete recombination of modal responses. On the other hand, Fig. 9 shows the same nodal power spectral densities as in Fig. 7, for the simplified variant "D-". It shows two important points: (i) energy in the response is lost with respect to the most general and complete variant "Ff-", coming from a loss of such energy at the level of modal loads; (ii) the compensation problem discussed above, which results in the flattening of the background (quasi-static) peak around the origin $\omega = 0$, particularly noticeable for the left-most midspan point (A).

In order to evaluate the influence of the modal correlation, two variants of the case with the full CPSM matrix of wind turbulences are considered : in variant "Ff-" modal recombinations are performed with the CQC and CCC (Ff standing for Full-full), while in variant "Fd-" the modal correlations are neglected both at second and third orders, which corresponds to the SRSS and CRSC combination methods (in that case, Fd stands for Full-diagonal).

Finally, Fig. 10 shows the peak factors as well as fluctuating parts of the extreme values of the vertical displacements. This Figure will serve for the discussion on the different modeling assumptions. It shows three categories of curves, each one corresponding to a different variant of modeling (D-, Fd- and Ff-). Then, for each variant, two

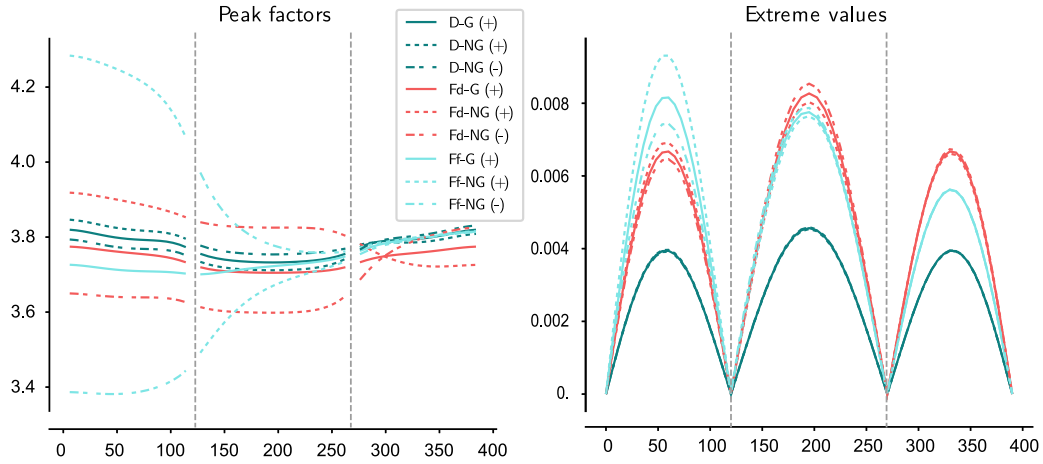

Fig. 10. Peak factors and fluctuating part of the extreme values of vertical structural displacements. Variants of the structural analysis are: D- (no coherence in wind loads, correlation of modal responses neglected), Ff- (coherent wind loading + complete combinations) and Fd- (coherent wind loading + SRSS/CRSC combinations). For each variant, the extreme values are computed with a Gaussian approach (-G), or with a non-Gaussian approach (-NG+ and -NG-).

different ways of computing the extreme values are shown : either with a Gaussian formulation (based on Rice's formula), either a non-Gaussian formulation (based on Kareem-Zhao formula), as explained in Section 6. In the case of a non-Gaussian peak factor, the upper and lower values might differ, so we provided the positive and negative extreme values. The extreme values represented in Fig. 10-b correspond to the peak factor multiplied by the standard deviations for each node. To these values, the average displacement field should be added but it is omitted here to ease the reading.

This illustration reveals several important points:

- the complete cubic combination is of primary importance in the determination of third statistical moments. Indeed, the maximum displacement in the left-most span in the two scenarios Ff-NG and Fd-NG results in a difference of about 26% (maximum vertical displacement of 0.0094 m vs. 0.007 m respectively). This is a consequence of the fact that there are proportionally more elements in the third order moment tensor with respect to the number of elements on the diagonal, than the same ratio for the covariance matrix. In other words, there are many more elements outside the main diagonal of the third order moment tensor so that, even if they are relatively small, they contribute to the third moment of structural responses.
- the simplified variant "D-" suffers from a difference of more than 50% with respect to the complete variant "Ff-", and between 40%–45% with the variant "Fd-" in the maximum vertical displacement in the left-most span, which maximum is of 0.004 m.
- the comparison of Ff-G and Fd-G doesn't show a large difference in terms of peak factors, but well in terms of extreme values (0.0082 m vs. 0.0065 m, i.e. a difference of 20%). This indicates that the SRSS and CQC combinations provide slightly different standard deviations.
- Fig. 10 confirms that the loading case of variant D- results in a nearly Gaussian process. This is observable since all three peak factors have very similar values and all three eigen values are virtually superimposed. This is explained by the central limit theorem as stated above.
- the analysis case that results in the largest peak factors is "Ff-", with a significant difference between the positive and the negative peak factors, which indeed translates into significantly different envelopes of extreme values (17% difference in absolute values).
- additionally, for scenarios Ff-, the responses in the central and right-most spans are also nearly Gaussian. This has already been underlined based on the power spectral densities and bispectra of the displacements in the mid-spans of those two spans. It is attributable to the fact that the response is mostly background in the left span, while it is mostly resonant in the two rightmost ones. This effect is slightly less remarked for the Fd- ones, since in such case the use SRSS+CRSC modal recombinations (instead of the CQC/CCC for Ff-, see Section 6) is not sufficient for a full compensation of effects.

All in all, this example shows the importance of a non-Gaussian (bispectral) analysis in such a case where part of the structure responds in a quasi-static manner. It also highlights the importance of a complete cubic recombination of modal responses as soon as higher order moments are estimated.

8.3. Influence of the number of POD modes

At the beginning of Section 7, the two possible extreme (and undesired) scenarios have been presented regarding the proposed methodology; (i) fast but inaccurate, or (ii) accurate but extremely slow. From the mathematical point of view, this is directly related to the kept number of wind modes N_p (and equivalently N_q) when applying the POD to the incoming wind field, as of (35). Indeed, use of dimensionality reduction techniques such as POD is of crucial interest when a given phenomenon can be accurately represented by means of a reduced number N_p of independent elements. However, in the results presented so far, all wind modes were considered, that is, $N_p \equiv \mathtt{NN}$. From a mathematical point of view, this is indeed equivalent to no POD application at all, since considering all wind modes does lead to no information loss. Nevertheless, even without any modal truncation, the computational cost decreases by a factor of order 10x, which becomes more and more significant as soon as the absolute time (e.g. problem size) increases (i.e. 10days vs. 1day). This speedup is indeed justified by the theoretical concepts that have been detailed in Section 5, which under a computational point of view, results in the possibility of precomputing some terms instead of having to compute them at each loop iteration. This alone has considerably contributed to prove how POD application in such context is very powerful. Specifically, for the problem considered here, CPU time has varied from about 6 min for $N_p = 1$, to 15 min for $N_p = 21$. The computational speedup does not increase linearly with the number of POD modes (i.e. around 9 min for the case with 9 POD modes). However, this saving might become remarkable for much larger problems.

In practice, there is no unique optimal value for the kept number of wind modes N_p. It is indeed case specific. Retaining between 80%–90%

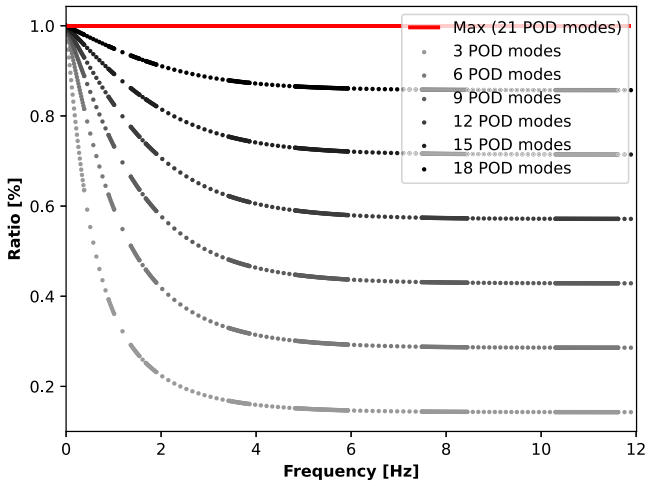

Fig. 11. Evolution of relative energy with frequency, with changing number of kept POD modes.

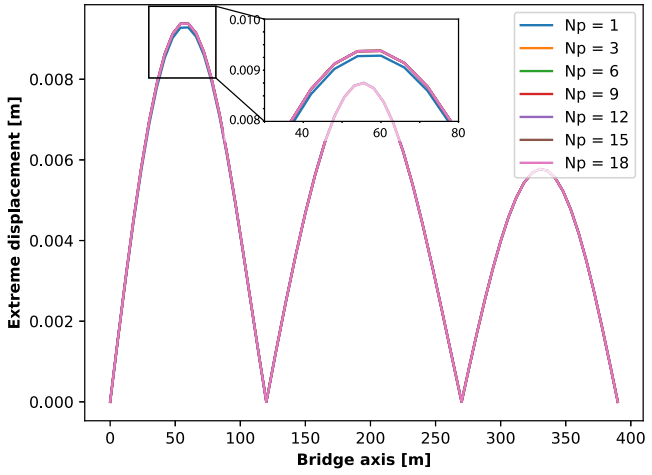

Fig. 12. Influence of the number of POD modes used in the analysis, on the maximum structural displacements.

of the wind energy might offer a good compromise between speed and accuracy. These ratios also seem to be current practice in other fields of application of POD.

Fig. 11 shows the ratio of energy contained in the trace of the matrix of eigenvalues of kept modes. Clearly, for the considered case, as soon as the frequency of the load increases, a higher number of POD modes is necessary in order to guarantee the same amount of energy with respect to lower frequencies. This is indeed justified by the fact that, being large scale turbulence and slow-varying process, the main frequency content is towards the lower spectrum of frequencies. As a consequence, in this range, a small number of POD modes already provides more than 70%–80% of the total energy. This trend soon vanishes as soon as we perform this evaluation at higher frequencies, where in this case, all modes tend to equally contribute to the representation of the loading field.

However, this concerns the wind loading only. Including the structure and investigating the load-structure interaction, one might find that actually, even less POD modes (or in some cases, not the most energetic ones) are the ones actually contributing to the final structural response. This is discussed in details in Carassale et al. (2001). Fig. 12 shows in fact how, for the studied example, already the first POD mode is almost entirely sufficient for accurately reconstructing the full structural response. From 3 to 18 POD modes, the resulting response does not change, meaning that 3 POD modes are the actual only POD modes sufficient to reconstruct the full structural response. Unfortunately however, this information is hardly known beforehand, leading the practitioner to a choice which would, and should, guarantee an adequate precision without having the need of performing the reference case (which would indeed invalidate all this reasoning).

9. Conclusion and future perspectives

In this paper, Higher-Order Stochastic Analysis is applied to a medium size realistic example for the first time. Particularly, the focus was on the exact numerical estimation of the skewness coefficient of structural displacements. The analysis of a medium size structure (366 DOFs) has been made possible thanks to the combination of (i) an optimized 2-stage meshing strategy that places integration points in the 2-D frequency space in such a way to use a minimum number of projections of the wind loading field in the modal basis, (ii) the use of a Proper Orthogonal Decomposition of the turbulent wind field. This second peculiarity of our approach is also a first extension of the so-called double modal transformation to higher order stochastic analysis.

Although the final goal targets applications to large real cases, this study focused on a medium-size problem which is presented in an academic format so that it could be used as a benchmark for other developers. This test case has the merit to mix responses of different types (background vs. resonant) and demonstrates the usefulness of a non-Gaussian analysis. The analysis of this structure could run within a couple of minutes on a regular desktop computer, while it would not have been possible to run the simulation without the POD reduction technique, for memory storage limitations. Computation runtime would also be an important issue, should the memory be sufficient.

The example has also allowed discussion about some variants of the complete analysis, revealing that the complete combinations of modal responses (CQC and Complete Cubic Combination) are required, but also that the spatial coherence of the wind loads is of primary importance for such a structure.

With this integrated non-Gaussian analysis framework, it is now possible to revisit the buffeting analysis of large structures of various types. Following steps could include unsteady (flutter-like) effects, although a full Non-Gaussian analysis would make less sense in that context where oscillations (symmetrical distributions) are expected. Another perspective of this work is its extension to fourth order analysis which would grant access to the first four statistical moments of the responses, and hence possible application of cubic translation methods for the estimation of peak factors.

CRediT authorship contribution statement

M. Esposito Marzino: Conceptualization, Methodology, Software, Validation, Investigation, Writing – original draft, Visualization. **V. Denoël:** Conceptualization, Methodology, Validation, Investigation, Writing – review & editing, Supervision, Project administration, Funding acquisition.

Declaration of competing interest

The authors declare that they have no known competing financial interests or personal relationships that could have appeared to influence the work reported in this paper.

Data availability

Data will be made available on request.

Acknowledgments

Part of this research project has been supported thanks to a research project funded by the Walloon Region (Convention Nb. 8096, FINELG2020).

References

Aas-Jakobsen, K., Strømmen, E., 2001. Time domain buffeting response calculations of slender structures. J. Wind Eng. Ind. Aerodyn. 89 (5), 341–364.

Augusti, G., Borri, C., Marradi, L., Spinelli, P., 1986. On the time-domain analysis of wind response of structures. J. Wind Eng. Ind. Aerodyn. 23, 449–463.

Benfratello, S., Caddemi, S., Muscolino, G., 2000. Gaussian and Non-Gaussian stochastic sensitivity analysis of discrete structural system. Comput. Struct. 78, 425–434.

Benfratello, S., Falsone, G., Muscolino, G., 1996. Influence of the quadratic term in the alongwind stochastic response of SDOF structures. Eng. Struct. 18, 685–695.

Canor, Thomas, Blaise, Nicolas, Denoël, Vincent, 2012. Efficient uncoupled stochastic analysis with non-proportional damping. J. Sound Vib. 331 (24), 5283–5291.

Carassale, Luigi, Piccardo, Giuseppe, Solari, Giovanni, 2001. Double modal transformation and wind engineering applications. Journal of Engineering Mechanics 127 (5), 432–439.

Carassale, L., Solari, G., 2002. Wind modes for structural dynamics: a continuous approach. Probabilistic Engineering Mechanics 17 (2), 157–166, https://www.sciencedirect.com/science/article/pii/S0266892001000364.

da Costa, Bernardo Morais, Wang, Jungao, Jakobsen, Jasna Bogunović, Øiseth, Ole Andre, þór Snæbjörnsson, Jónas, 2022. Bridge buffeting by skew winds: A quasi-steady case study. J. Wind Eng. Ind. Aerodyn. 227, 105068.

Davenport, Alan Garnett, 1961. The application of statistical concepts to the wind loading of structures. Proc. Inst. Civ. Eng. 19 (4), 449–472.

Denoël, Vincent, 2009. Polynomial approximation of aerodynamic coefficients based on the statistical description of the wind incidence. Probab. Eng. Mech. 24 (2), 179–189.

Denoël, Vincent, 2011. On the background and biresonant components of the random response of single degree-of-freedom systems under non-Gaussian random loading. Eng. Struct. 33 (8), 2271–2283.

Denoël, Vincent, 2012. Extension of the background/biresonant decomposition to the estimation of the kurtosis coefficient of the response. In: Uncertainty in Structural Dynamics.

Denoël, Vincent, 2015. Multiple timescale spectral analysis. Probab. Eng. Mech. 39, 69–86.

Denoël, Vincent, Carassale, Luigi, 2014. Efficient estimation of the high-order response statistics of a wind-excited oscillator with nonlinear velocity feedback. In: INVento.

Denoël, Vincent, Degée, Hervé, 2009. Asymptotic expansion of slightly coupled modal dynamic transfer functions. J. Sound Vib. 328 (1–2), 1–8.

Denoël, Vincent, Maquoi, René, 2012. The concept of numerical admittance. Arch. Appl. Mech. 87, 1337–1354.

Denoël, V., Marzino, M. Esposito, Geuzaine, M., 2023. A multiple timescale approach of bispectral correlation. Journal of Wind Engineering and Industrial Aerodynamics 232, 105282.

Fan, Wenliang, Sheng, Xiangqian, Li, Zhengliang, Sun, Yi, 2022. The higher-order analysis method of statistics analysis for response of linear structure under stationary non-gaussian excitation. Mech. Syst. Signal Process. 166, 108430.

Flamand, Olivier, Denoël, Vincent, 2011. Influence of bridge deck shape on extreme buffeting forces. In: Proceedigs of 13th International Conference on Wind Engineering.

Geuzaine, Margaux, Denoël, Vincent, 2019. A framework for the efficient spectral analysis of large wind-and wave-loaded structures. In: 15th International Conference on Wind Engineering.

Gioffrè, Massimiliano, Gusella, Vittorio, Mircea, Grigoriu, 2001. Non-Gaussian wind pressure on prismatic buildings. Struct. Eng. 127, 981–989.

Gurley, Kurtis R., Tognarelli, Michael A., Kareem, Ahsan, 1997. Analysis and simulation tools for wind engineering. Probab. Eng. Mech. 12 (1), 9–31.

Gusella, Vittorio, Materazzi, Annibale Luigi, 1998. Non-Gaussian response of MDOF wind-exposed structures: Analysis by bicorrelation function and bispectrum. Meccanica 33, 299–307.

Gusella, Vittorio, Materazzi, Annibale Luigi, 2000. Non-Gaussian along-wind response analysis in time and frequency domains. Eng. Struct. 22, 49–57.

Holmes, John D., 1981. Non-Gaussian characteristics of wind pressure fluctuations. J. Wind Eng. Ind. Aerodyn. 7, 103–108.

Isyumov, Nicholas, 2012. Alan G. Davenport's mark on wind engineering. J. Wind Eng. Ind. Aerodyn. 104, 12–24.

Janjic, Dorian, Pircher, Heinz, 2004. Consistent numerical model for wind buffeting analysis of long-span bridges. In: IABSE Symposium Report, Vol. 88. International Association for Bridge and Structural Engineering, pp. 78–83.

Kareem, Ahsan, 1984. Nonlinear wind velocity term and response of compliant offshore structures. Eng. Mech. 110, 1573–1578.

Kareem, A. al, Tognarelli, M.A., Gurley, K.R., 1998. Modeling and analysis of quadratic term in the wind effects on structures. J. Wind Eng. Ind. Aerodyn. 74, 1101–1110.

Kareem, Ahsan, Wu, Teng, 2013. Wind-induced effects on bluff bodies in turbulent flows: Nonstationary, non-Gaussian and nonlinear features. J. Wind Eng. Ind. Aerodyn. 122, 21–37.

Kimura, K., Tanaka, H., 1992. Bridge buffeting due to wind with yaw angles. J. Wind Eng. Ind. Aerodyn. 42 (1–3), 1309–1320.

Kwon, Dae-Kun, Kareem, Ahsan, 2009. Peak factor for non-Gaussian processes revisited. In: The Seventh Asia-Pacific Conference on Wind Engineering.

Lutes, Loren D., Sarkani, Shahram, 2004. Random Vibrations: Analysis of Structural and Mechanical Systems. Butterworth-Heinemann.

Mircea, Grigoriu, 1995. Linear systems subject to non-Gaussian α-stable processes. Probab. Eng. Mech. 10, 23–34.

Rizzi, Stephen A., Przekop, Adam, Turner, Travis L., 2011. On the response of a nonlinear structure to high kurtosis non-Gaussian random loadings. In: EURODYN2011-8th International Conference on Structural Dynamics. number NF1676L-10853.

Scanlan, Robert H., 1993. Bridge buffeting by skew winds in erection stages. J. Eng. Mech. 119 (2), 251–269.

Simiu, Emil, Scanlan, Robert H., 1996. Wind Effects on Structures: Fundamentals and Applications to Design, Vol. 688. John Wiley, New York.

Solari, Giovanni, 2020. Thunderstorm downbursts and wind loading of structures: progress and prospect. Frontiers in Built Environment 6, 63.

Solari, Giovanni, Carassale, Luigi, Tubino, Federica, 2007. Proper orthogonal decomposition in wind engineering - Part 1: A state-of-the-art and some prospects. Wind Struct. 10 (2), 153–176.

Solari, Giovanni, De Gaetano, Patrizia, 2018. Dynamic response of structures to thunderstorm outflows: Response spectrum technique vs time-domain analysis. Eng. Struct. 176, 188–207.

Trapp, Arvid, Wolfsteiner, Peter, 2019. Characterizing non-Gaussian vibration loading using the trispectrum. In: Journal of Physics: Conference Series, Vol. 1264. IOP Publishing, 012040.